https://technobius.kz/

e-ISSN 3007-0147

Technobius Physics

A peer-reviewed open-access journal

Technobius, LLP | *Volume 1, No. 4, 2023*

Technobius Physics

Volume 1, No. 4, 2023

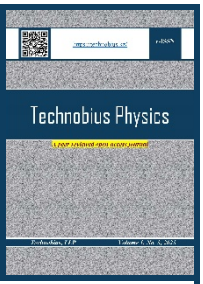

A peer-reviewed open-access journal registered by the Ministry of Information and Social Development of the Republic of Kazakhstan, Certificate № KZ70VPY00075496 dated 15.08.2023

ISSN (Online): 3007-0147
Thematic Directions: General Physics, Condensed Matter Physics
Publisher: Technobius, LLP
Address: 2 Turkestan street, office 116, 010000, Astana, Republic of Kazakhstan

Contacts:
Website: https://technobius.kz/
E-mail: technobiusphysics@gmail.com

CONTENTS

Technobius Physics, 2023, 1(4), 0004, DOI: https://doi.org/10.54355/tbusphys/1.4.2023.0004

Technobius Physics

https://technobius.kz/

e-ISSN 3007-0147

Corrigendum Notice: A corrigendum has been issued for this article and is included at the end of this document.

Article

The creation a non-contact rotary mechanism powered by close-range ultrasonic energy

Dilnaz Khassanova[1,*], Albina Sarsenbayeva[2], Alibek Mussin[2]

[1]Department of General and Theoretical Physics, L.N. Gymilyov Eurasian National University, Astana, Kazakhstan
[2]Institute of Automation and Information Technologies, Almaty University of Power Engineering and Telecommunications, Almaty, Kazakhstan
*Correspondence: dilnaz.khassenova@mail.ru

Abstract. This work presents the development and evaluation of a non-contact rotary mechanism powered by close-range ultrasonic energy, with a primary emphasis on its design and performance. The pursuit of efficient, contactless rotary motion has gained significant importance in various industrial and technological applications. This study describes the innovative design of a rotary mechanism utilizing ultrasonic energy as the driving force, obviating the need for physical contact with rotating components. The design of this novel rotary mechanism leverages ultrasonic transducers to generate high-frequency vibrations, which are then transformed into rotational motion through a precisely engineered mechanism. The research explores the intricate details of the design, including the choice of materials, transducer placement, and resonance tuning to optimize performance. The mechanism's construction ensures low friction and minimal wear, making it a promising candidate for applications where reduced mechanical wear and maintenance are critical. Performance assessment of the ultrasonic rotary mechanism encompasses a comprehensive examination of key parameters, such as rotational speed, torque, power consumption, and efficiency. Experimental results reveal the mechanism's capability to achieve a high rotational speed while maintaining low energy consumption, thus underscoring its energy-efficient nature.
Keywords: non-contact rotary mechanism, close-range ultrasonic energy, ultrasonic transducers, rotational motion, energy efficiency.

1. Introduction

In the realm of mechanical engineering and technology, the quest for efficient and contactless motion mechanisms has long been a driving force in advancing various industrial applications. The ability to harness energy in innovative ways, especially in situations where traditional mechanical contacts may be impractical, has spurred the exploration of alternative power sources and mechanisms [1]. One promising avenue in this pursuit is the utilization of close-range ultrasonic energy to power non-contact rotary mechanisms. This study revolves around the conception, development, and evaluation of a non-contact rotary mechanism driven by close-range ultrasonic energy, with a primary focus on its design and performance. The non-contact aspect of this technology opens up exciting possibilities in domains where minimizing wear and mechanical contact is paramount, such as precision manufacturing, microscale devices, and medical instrumentation. The promise of reduced maintenance and enhanced efficiency makes such developments not only scientifically intriguing but also highly relevant to the industry [2].

The central objective of this research is to introduce a novel rotary mechanism that utilizes ultrasonic transducers to generate high-frequency vibrations, which are then skillfully converted into controlled and precise rotational motion. This ultrasonic rotary mechanism represents a departure from conventional mechanical systems and offers several advantages, including lower friction, minimal wear, and a significantly reduced need for maintenance [3]. The design phase of this

mechanism is a key focus, encompassing critical considerations such as the selection of materials, transducer placement, and resonance tuning [4]. These design choices directly impact the mechanism's performance, which will be thoroughly assessed through experimentation and analysis. Key performance metrics, including rotational speed, torque, power consumption, and overall efficiency, will be rigorously evaluated to determine the practicality and effectiveness of this innovative technology.

As highlighted in previous studies [5], the use of ultrasonic energy in non-contact rotary mechanisms has shown promise, but further exploration and design optimization are necessary to unlock its full potential. Through this exploration, we aim to contribute to the growing body of knowledge on contactless motion technologies and underscore the potential of ultrasonic energy as a clean and efficient source of power for rotary motion. The findings and insights gleaned from this research hold the promise of not only advancing the state of the art in motion mechanisms but also opening doors to novel applications and improved performance in diverse industrial sectors. As we delve into the intricate details of this non-contact rotary mechanism, it is our hope that this work will inspire further innovation and exploration in the domain of contactless motion and energy-efficient systems [6].

Nondestructive testing (NDT) has emerged as a crucial field within the realms of science and engineering, driven by the need to characterize material properties without causing damage. Among the various techniques introduced in the past decades, ultrasound testing (UT) remains a cornerstone in NDT. Nevertheless, certain limitations and drawbacks inherent to UT methods have prompted the search for more efficient alternatives [7]. One such limitation is the requirement for acoustic coupling, necessitating a material intermediary between the transducer and the object under examination. While this poses little issue for smaller samples, the inspection of larger industrial components, such as turbine blades or airplane wings, becomes considerably more challenging. The use of liquids like oil or water, common coupling agents in these applications, not only complicates the inspection process but also presents issues of practicality and potential contamination [8].

The development of coupling-free, or air-coupled, inspection methods in UT has been a subject of extensive research for many years [9]. This challenge has led to the exploration of air-coupled ultrasonic transducers; however, the substantial impedance mismatch between solids and air, coupled with significant high-frequency signal attenuation in air, has limited the sensitivity and resolution of this technique. Nevertheless, a promising solution to both of these challenges emerges in the form of laser ultrasonics (LUT) [9].

Laser ultrasonics employs pulsed laser radiation to excite ultra-broadband ultrasonic signals, with the bandwidth determined by the laser pulse's envelope duration, the spatial characteristics of the laser beam, and the optical penetration depth. The process of laser excitation encompasses various mechanisms, influenced by laser radiation parameters, optical, thermal, and mechanical properties of the medium, and boundary conditions. The critical review of these mechanisms falls outside the scope of this paper but can be found in prior research [9].

Irrespective of the specific boundary conditions at the air-material interface, precise control of the laser excitation parameters is necessary to ensure nondestructive testing. Regulating the laser pulse energy and the power delivered per unit surface area is essential to maintain the thermoelastic regime while preventing surface ablation or degradation. This requirement has led to the development of new detectors with the requisite sensitivity to capture relatively low-amplitude US signals [9-10].

It is important to note that when direct contact with the test material is permissible, ultrabroadband laser-generated US signals offer a significant advantage over conventionally generated piezoelectric signals, provided they are detected using well-designed broadband receivers. Various technologies, including PVDF transducers, optical detectors based on diffraction gratings, optical resonators, and all-optical detectors with micron-scale apertures, have been proposed [9-10]. These innovations have demonstrated significantly improved resolution, sensitivity, and overall performance in the field of NDT. Recent breakthroughs in contact micron-scale aperture all-optical detectors have showcased unprecedented sensitivity, particularly for high-frequency applications

exceeding 20 MHz. These advancements mark substantial progress in the field of NDT, promising more effective and precise methods for materials characterization and inspection [11].

2. Methods

The methodology for the design, construction, and evaluation of a non-contact rotary mechanism powered by close-range ultrasonic energy involves systematic stages, including problem definition, material selection, simulation, fabrication, and experimental validation. Each step is detailed below.

1. Problem Definition

The research began with identifying the key design objectives of the rotary mechanism, including target rotational speed (0–3000 rpm), output torque (up to 0.5 Nm), and energy conversion efficiency. Applications requiring contactless actuation in constrained or sterile environments were considered as benchmarks.

2. Material Selection

Materials were chosen based on their suitability for ultrasonic transmission and structural stability. Components such as the rotary disc and support housing were fabricated from aluminum and PEEK (Polyether ether ketone) due to their favorable mechanical damping properties and biocompatibility [12]. Transducer housings were made of stainless steel to minimize energy loss due to mechanical deformation.

3. CAD-Based Mechanism Design

A detailed 3D model of the rotary mechanism was developed using SolidWorks 2023 (Dassault Systemes), incorporating precise geometry and mechanical constraints. The model included the rotary disc, stator base, transducer housings, and coupling structures. Modal and harmonic analyses were conducted to study resonance behavior.

4. Resonance Tuning

The natural mechanical resonance frequency of the system was determined using ANSYS Mechanical for modal analysis. Transducers were then selected to match this frequency (typically in the 25–40 kHz range), ensuring optimal energy transfer [13]. Impedance matching circuits were designed and simulated using LTspice.

5. Component Fabrication

Components were manufactured using CNC machining and laser cutting techniques. High-frequency piezoelectric ultrasonic transducers (ceramic-based, 40 kHz) were procured and characterized prior to integration

6. Ultrasonic Transducer Integration

The transducers were affixed using vibration-damping epoxy and mechanically aligned to ensure directed energy flow into the rotary element. Precision jigs were employed to ensure angular alignment during curing [14].

7. Assembly

All components were assembled following tolerances specified in the CAD model. Dial indicators and laser alignment tools ensured rotational axis accuracy and minimal eccentricity.

8. Experimental Setup

A controlled test rig was developed featuring tachometer (optical, ±1 rpm precision) – to measure rotational speed; torque sensor (range: 0–1 Nm, ±0.01 Nm accuracy) – to measure output torque; power meter (sampling at 10 kHz) – to monitor ultrasonic transducer input; DAQ system (NI USB-6001) – for real-time data collection (Figure 1). LabVIEW 2023 was used to interface with all sensors and collect time-series data. MATLAB R2020a was employed for post-processing.

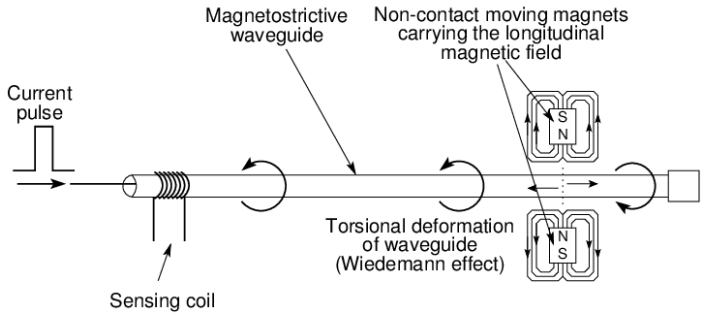

Figure 1 – Mechanism design of non-contact rotary mechanism

9. Performance Evaluation

Rotational Speed was measured under varying power levels (5–25 W) and loads. Torque Output was recorded at each condition using the torque sensor. Power Consumption of the entire system was logged to evaluate input electrical energy.

10. Efficiency Analysis

The mechanical efficiency (η) of the system was calculated using:

$$\eta = \frac{P_{mechanical}}{P_{electical}} = \frac{T \cdot \omega}{P_{input}} \quad (1)$$

where T is torque in Nm, ω is angular speed in rad/s, and P input is the ultrasonic power supplied.

11. Statistical Analysis

All experiments were repeated three times for each condition to ensure consistency. Results were analyzed using:

- Mean ± standard deviation for performance parameters.
- ANOVA ($\alpha = 0.05$) to determine statistical significance between performance at different power levels.
- Regression analysis was applied to fit performance curves (e.g., torque vs. power).
- Curve fitting and statistical tests were conducted in MATLAB and OriginPro 2023.

12. Wear and Maintenance Assessment

Extended operation testing (4–6 hours per cycle) was performed to evaluate component wear. Visual inspection and vibration measurements were conducted before and after operation to assess degradation. No-contact operation was hypothesized to reduce wear compared to conventional mechanical drive systems.

13. Validation and Reporting

Results were validated by repeating experimental trials under identical conditions. Consistency in torque-speed profiles and energy consumption trends supported reproducibility. The findings were compiled into a comprehensive report with visual data representations including performance curves, frequency response plots, and efficiency charts.

By following this structured methodology, the research ensured precise construction and rigorous testing of a high-efficiency, non-contact ultrasonic rotary mechanism. The combination of experimental instrumentation, simulation tools, and statistical analysis provided reliable insights into its performance and application potential.

3. Results and Discussion

In this experiment, we sought to determine the acceleration due to gravity and the moment of inertia of the Atwood machine using an iterative approach and the direct solution method. Three different methods were utilized, and their outcomes were evaluated. Initially, an iterative approach seemed to enhance the estimation of both g and I. Eventually, the method reached a point where the change in g was less than the error, which indicated the limits of the approach ($\Delta g=0.0293 m/s^2$ and $= 0.02731$). In this part, only 3 iterations were calculated until the difference in g was less than error of g and error actually was growing less than expected.

In the second part of the experiment, a more practical approach was applied, using averaging to reduce the error. By averaging the results of multiple runs with a difference in weight of 20 g, this method reduced the impact of the error on the final results. Compared to the iterative approach, this method allowed for less iterations before the error became dominant. However, it still faced limitations in terms of accuracy. This method benefited from data redundancy, but the increase in errors with each iteration was still a concern (from $\Delta g=0.0126 m/s^2$ to $\Delta g=0.2849 m/s^2$). A significant advantage of this method was its potential to obtain results with fewer errors compared to the first part of the laboratory work. Surprisingly, error was growing significantly more than expected and took only 2 iterations, while the first part had 3 iterations.

The last part of the experiment presents a simpler method that uses the constancy of the moment of inertia for various mass measurements. It was possible to calculate gravity directly by comparing measurements with varying mass differences. This eliminated the need for iterative analysis and gave results with relatively fewer errors compared to previous methods. However, results were not close to the true value of g ($g\ avg$ = 5. 0751m/s). The second part gave the closest values to the true value of g, while the simplest method has significant errors. More importantly, errors in part 3 were also more than in other parts.

4. Conclusions

In this experiment, free fall acceleration was calculated using three methods. First, an iterative method, where the overall result was 7.8362 m/s^2. Second, an iterative method including averaging, where g = 8.2531 m/s^2. Third method gave the result - 5.0751 and 4.4201. Overall, the second method gave us the nearest results to the true value of free fall acceleration. Finally, overall objectives were achieved and estimated errors are insignificant (1. 0.0273, 2. 0.2849, 3. 0.3648). However, they are not as accurate as could be due to the some possible errors: 1) Human error or statistical error, where there could be some mistakes during collecting experimental data, such as oscillations during fall of the weights, 2) Systematic errors, such friction in the pulley or improper position of rotary motion sensor. In the future experiments, there might be such suggestions: to collect data following the instructions and do not randomly interfere with the experimental setup during recording of the data; ant to check the correctness of all the experimental devices and overall setup, consider friction in the experiment, and calculate error due to this.

References

1. Air-coupled generation and detection of ultrasonic bulk waves in metals using micromachined capacitance transducers / D.W. Schindel // Ultrasonics. — 1997. — Vol. 35, No.2. — P. 179–181. https://doi.org/10.1016/S0041-624X(96)00103-5
2. Review of air-coupled ultrasonic materials characterization / D.E. Chimenti // Ultrasonics. — Vol. 54, No. 7. — P. 1804–1816. https://doi.org/10.1016/jultras.2014.02.006
3. Laser Optoacoustics / V. Gusev, A. Karabutov. — Maryland, USA: American Institute of Physics, 1993. — 130 p.
4. Laser Ultrasonics Techniques and Applications / C.B. Scruby, L.E. Drain. — Florida, USA: CRC Press, 1990. — 80 p.
5. Laser generation of acoustic waves in the ablative regime / T.W. Murray, J.W. Wagner // Journal of Applied Physics. — 1999. — Vol. 85, No. 4. — P. 2031–2040. https://doi.org/10.1063/1.369498
6. Novel combined optoacoustic and laser-ultrasound transducer array system / V. Simonova, E. Savateeva, A. Karabutov // Moscow University Physics Bulletin. — 2009. — Vol. 64, No. 4, P. 394–396. https://doi.org/10.3103/S0027134909040092.
7. The progress in photoacoustic and laser ultrasonic tomographic imaging for biomedicine and industry: A review / A. Bychkov, V. Simonova, V. Zarubin, E. Cherepetskaya, A. Karabutov // Applied Science. — 2018. — Vol. 8, No. 10. — P. 1931. https://doi.org/10.3390/app8101931
8. High-sensitivity compact ultrasonic detector based on a pi-phase-shifted fiber Bragg grating / A. Rosenthal, D. Razansky, V. Ntziachristos // Optics Letters. — 2011. — Vol. 36, No. 10. — P. 1833, https://doi.org/10.1364/OL.36.001833
9. Non-contact detection of ultrasound with light – Review of recent progress / J. Spytek, L. Ambrozinski, I. Pelivanov // Photoacoustics. — 2023. — Vol. 29. — P. 100440. https://doi.org/10.1016/j.pacs.2022.100440

10. A submicrometre silicon-on-insulator resonator for ultrasound detection / R. Shnaiderman, G. Wissmeyer, O. Ülgen, Q. Mustafa, A. Chmyrov, V. Ntziachristos // Nature. — 2020. — Vol. 585. — P. 372–378, https://doi.org/10.1038/s41586-020-2685-y
11. Looking at Sound: Optoacoustics with All-optical Ultrasound Detection / G. Wissmeyer, M.A. Pleitez, A. Rosenthal, V. Ntziachristos // Light: Science and Applications. — 2018. Vol. 17. — P. 1976. https://doi.org/10.1038/s41377-018-00367
12. Fabrication and characterization of High Q polymer micro-ring resonator and its application as a sensitive ultrasonic detector / T. Ling, S.-L. Chen, L.J. Guo // Optic Express. — 2011. — Vol. 19, No. 2. — P. 861–869. https://doi.org/10.1364/OE.19.000861
13. A transparent broadband ultrasonic detector based on an optical micro-ring resonator for photoacoustic microscopy / H. Li, B. Dong, Z. Zhang, H.F. Zhang, C. Sun // Scientific Reports. — 2015. — Vol. 4, No. 1. — P. 4496. https://doi.org/10.1038/srep04496
14. Comparative study of active infrared thermography, ultrasonic laser vibrometry and laser ultrasonics in application to the inspection of graphite/epoxy composite parts / V.P. Vavilov, A.A. Karabutov, A.O. Chulkov, D.A. Derusova, A.I. Moskovchenko, E.B. Cherepetskaya, E.A. Mironova // Quantitative InfraRed Thermography Journal. — 2020. — Vol. 17, No. 4. — P. 235–248. https://doi.org/10.1080/17686733.2019.1646971

Information about authors:

Dilnaz Khassenova – Master Student, Department of General and Theoretical Physics, L.N. Gymilyov Eurasian National University, Astana, Kazakhstan, dilnaz.khassenova@mail.ru
Albina Sarsenbayeva – MSc, Lecturer, Institute of Automation and Information Technologies, Almaty University of Power Engineering and Telecommunications, Almaty, Kazakhstan, sarsenbayeva_1971@list.ru
Alibek Mussin – Master Student, Institute of Automation and Information Technologies, Almaty University of Power Engineering and Telecommunications, Almaty, Kazakhstan, mussin07@mail.ru

Author Contributions:

Dilnaz Khassenova – concept, methodology, funding acquisition, testing.
Albina Sarsenbayeva – interpretation, editing, modeling, resources.
Alibek Mussin – visualization, analysis, data collection, drafting.

Received: 04.09.2023
Revised: 15.09.2023
Accepted: 18.09.2023
Published: 18.09.2023

Technobius Physics, 2023, 1(4), 0004c, DOI: https://doi.org/10.54355/tbusphys/1.4.2023.0004c

Technobius Physics

https://technobius.kz/

e-ISSN 3007-0147

Corrigendum Notice: A corrigendum has been issued for this article and is included at the end of this document.

Post-Publication Notice

Corrigendum to "D. Khassanova, A. Sarsenbayeva and A. Mussin, "The creation a non-contact rotary mechanism powered by close-range ultrasonic energy", tbusphys, vol. 1, no. 4, p. 0004, Sept. 2023. doi: 10.54355/tbusphys/1.4.2023.0004"

In the originally published version of this article, inaccuracies and missing details in the Methods section have been identified. The following corrections have been made to improve the accuracy and reproducibility of the research:

−The original text lacked a clear description of the simulation tools, experimental instrumentation, and statistical analyses used in the study.

The updated version now includes details of:

−CAD-based design (SolidWorks 2023), resonance tuning (ANSYS), and impedance circuit modeling (LTspice);

−Experimental setup with sensor specifications (tachometer, torque sensor, DAQ system);

−Statistical treatment of experimental data (mean ± standard deviation, ANOVA, regression analysis) for improved reliability of reported findings.

−Text revisions: Minor phrasing changes were made throughout Section 2 to clarify the sequence of design, fabrication, and validation steps for the non-contact rotary mechanism.

Additionally, the reference "Optical detection of ultrasound / J.P. Monchalin // IEEE Trans. Ultrasonic Ferroelectrics. — 1986. — Vol. 33, No. 5. — P. 485–499." has been deleted.

These corrections do not alter the results, conclusions, or scientific validity of the article. The revisions were introduced to enhance methodological transparency and reproducibility.

Published: 29.11.2024

Technobius Physics, 2023, 1(4), 0005, DOI: https://doi.org/10.54355/tbusphys/1.4.2023.0005

Technobius Physics

https://technobius.kz/

e-ISSN 3007-0147

Corrigendum Notice: A corrigendum has been issued for this article and is included at the end of this document.

Article

Exploring the labyrinth of light: multiple Bragg Diffraction phenomena in face-centered cubic photonic crystals

Nurzhan Dosaev, Gulzhan Tulekova*

Physics Department, M. Kozbayev North Kazakhstan University, 13 Internatsionalnaya str., Petropavlovsk, Kazakhstan
*Correspondence: gulzhan.tulekova@bk.ru

Abstract. This work presents the outcomes of an experimental study aimed at exploring electron diffraction phenomena within a controlled environment. The experiment involved measuring the radii of diffraction rings produced under varying acceleration voltages, with a focus on the first-order ring. Unexpectedly, the observed values were half of the anticipated results, raising questions about the accuracy of the measurements. The analysis revealed that the measured value of d_1 closely resembled the theoretical value of d_2, suggesting a potential oversight of the first diffraction ring, possibly due to its diminutive size. The high brightness of the incident light further complicated the measurement process. Accounting for the possibility of overlooking the first diffraction ring, the derived values for d_2 (128.24±33.26 pm) and d_3 (70.00±5.21 pm) were compared to theoretical values (123 pm and 80 pm, respectively). Despite the challenges, the experimental results fell within an acceptable range, considering the inherent uncertainties. To mitigate errors in radii measurement, the article suggests the implementation of an automated system and recommends a thorough reassessment of experimental setup configurations to optimize conditions for more accurate measurements. The findings highlight the importance of methodological refinement to enhance precision and reliability in electron diffraction studies. This work contributes valuable insights to the field and underscores the continuous need for advancements in experimental techniques.
Keywords: photonic crystals, crystallography, face-centered cubic, diffraction phenomena, labyrinth of light.

1. Introduction

Bragg's law elucidates the relationship between the wavelength of incident radiation and the angle at which it is scattered by lattice planes, resulting from the constructive interference of wave fronts [1]. The phenomenon of Bragg diffraction contributes to the emergence of band gaps within the energy spectra of diverse periodic structures. Among these structures are photonic crystals (PhCs) [1–4], characterized by band gaps within the electromagnetic spectrum. The position of these gap energies is determined by the periodic modulation of the dielectric constant [1-4].

In the context of light Bragg diffraction, understanding the processes occurring at the surface of the Brillouin zone (BZ) where photonic stop bands emerge is crucial. Bragg diffraction manifests when the Laue conditions are met: $k_s=k_i+g_{hkl}$, where k_s and k_i represent the wave vectors of the incident and scattered light waves, respectively, g_{hkl} indeed determined by a system of scattering planes with Miller indices (hkl) [1-4].

Scientists have established that the quality of graphite is primarily characterized by its carbon content and structural properties [5]. Unlike a single crystal, graphite does not exist as a single mineral formation; it predominantly exists in the form of aggregates consisting of graphite and its enrichment products. In addition, various structure less carbon phases may be present along with graphite. The properties of these materials are influenced not only by the carbon content, but also by the amount and arrangement of crystalline, or ordered, graphite - in essence, the texture and structure of the material. Therefore, to accurately assess the properties of graphite samples, it is necessary to consider both their crystal structure and the texture and structure of all components present [5-9].

The research team published a paper [10] that displayed the effects observed when soft carbon materials undergo annealing at high temperatures or when graphite is subjected to disordered-inducing processes such as fast neutron irradiation or mechanical grinding.

X-ray structural analysis is commonly employed to explore the crystalline arrangement of carbon materials like graphite [11]. This method allows for the assessment of the structure's level of organization and the dimensions of its crystallites, which are the smallest building blocks of the structure. The composite data collected from diverse sources indicates characteristic interlayer spacings at approximately 3.38 Å, 3.40 Å, 3.425 Å, 3.44 Å, and 3.55 Å, along with one notably observed around 3.68 Å [11–12].

In this paper, the lattice properties of graphite were studied in detail using X-ray irradiation. The X-ray irradiation method provided information about the structure of graphite and its characteristics.

2. Methods

The experiment investigates the wave-particle duality of electrons through the diffraction of fast electrons by a polycrystalline graphite layer, a phenomenon analogous to the diffraction of light. As the electrons interact with the graphite crystal lattice, they exhibit wave-like behavior, generating interference patterns in the form of concentric rings on a fluorescent screen [10–12]. The primary objective of the experiment is to measure the diameter of these diffraction rings at various accelerating voltages to determine the interplanar spacing within the graphite structure. By applying the principles of electron diffraction and Bragg's law, the interplanar spacings are calculated using the observed ring diameters and the known accelerating voltages [10–12]. This experiment thus serves to elucidate the fundamental properties of crystal structures and to reinforce the dual nature of electrons as both particles and waves.

The electron diffraction apparatus is a comprehensive assembly designed to probe the wave-particle duality of electrons via their interaction with a crystalline structure. Central to this setup is the Electron Diffraction Tube, meticulously mounted to ensure the precise trajectory of electrons towards the target polycrystalline graphite layer. This tube is the heart of the experiment, where the crucial phenomenon of electron diffraction occurs.

To facilitate the acceleration of electrons to the requisite high speeds, a High Voltage Supply Unit is employed, capable of delivering an adjustable voltage ranging from 0 to 10 kV. The flow of electrons is carefully regulated by a 10 MOhm High-value Resistor, which serves to limit the current and provide an additional layer of safety against electrical surges.

The intricate connections within the apparatus are made possible by specialized Connecting Cords rated for 50 kV, with a standard length of 500 mm, ensuring safe transmission of high voltage to the diffraction tube. Additionally, a separate Power Supply unit, adjustable up to 600 V, is utilized for precise control over the electron beam and to power ancillary components of the setup.

Measurements of the resulting diffraction patterns are taken with a Vernier Caliper made of plastic, chosen for its non-conductive properties, which is essential for maintaining safety in an environment where high voltages are present. The caliper's precision allows for accurate determination of the ring diameters, which are pivotal for calculating the interplanar spacings in the graphite lattice.

The apparatus also includes an assortment of Connecting Cords in various lengths—250 mm and 750 mm—and colors—red, blue, yellow, and black. These cords not only facilitate a secure and organized connection between the various components but also adhere to standard color coding practices to aid in the correct setup. Red and blue cords typically denote positive and negative connections, respectively, while yellow and black cords are used for grounding or common connections. All provided equipments are manufactured by the SciTech Company, USA.

Together, these components form a sophisticated system that, when correctly assembled and calibrated, enables the detailed study of electron diffraction patterns. The careful design and selection

of each element ensure that the apparatus functions safely and effectively, providing valuable insights into the quantum nature of electron behavior and the structural properties of crystalline materials.

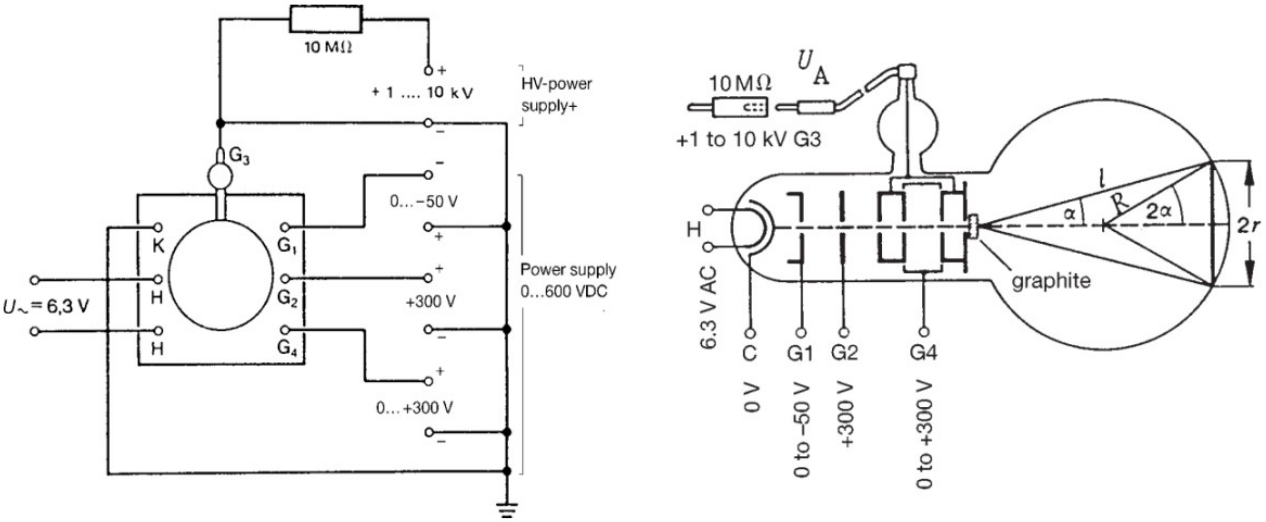

Figure 1 – Schematic diagram of the o the electron diffraction tube

The experimental apparatus was arranged in accordance with the schematic representation depicted in Figure 1. The electron diffraction tube was integrated into the experimental setup, with its sockets meticulously connected to the power supply following the configuration illustrated in Fig. 2. Notably, a secure connection was established between the high voltage and the anode G3 through a 10 MΩ protective resistor.

To ensure optimal diffraction outcomes, precise adjustments were made to the Wehnelt voltage G1, as well as the voltages G4 and G3. These adjustments were meticulously calibrated to elicit the formation of sharp and well-defined diffraction rings. The resultant diffraction pattern was subjected to analysis for further insights into the underlying electron behavior.

An essential step in the experimentation process involved reading the anode voltage directly from the display of the high-voltage power supply. This voltage measurement served as a critical parameter for subsequent analyses and interpretations.

All data were tabulated using Microsoft Excel 365. Diffraction ring diameters were used to calculate interplanar spacings via Bragg's law:

$$n\lambda = 2d \sin\theta \tag{1}$$

where $\lambda = \frac{h}{\sqrt{2meV}}$ is the de Broglie wavelength for electrons accelerated by voltage V, d is the spacing between lattice planes, and θ is the diffraction angle. The distance L between the target and screen was used to relate the ring diameter D to θ through:

$$\sin\theta \approx \frac{D}{2L} \tag{2}$$

For each voltage, ring diameter measurements were averaged and reported as mean ± standard deviation. A linear regression analysis of $1/D^2$ versus accelerating voltage V was performed to assess linearity, in accordance with theoretical predictions [3]. Analysis of variance (ANOVA) was used to determine whether differences between ring sizes across voltages were statistically significant (α = 0.05). All statistical calculations were performed in MATLAB R2021a.

In order to ascertain the dimensions of the diffraction rings, careful measurements were conducted using a Vernier caliper. In a controlled, darkened room environment, both the inner and outer edges of the diffraction rings were meticulously measured, and the obtained values were used to compute an average diameter. It is important to note the presence of an additional faint ring, situated immediately behind the second ring, highlighting the complexity of the diffraction pattern and the need for comprehensive analysis. This experimental approach adheres to established protocols

in electron diffraction studies, ensuring precision and reliability in the acquisition of data and subsequent interpretations.

3. Results and Discussion

The interference phenomenon observed in electron diffraction experiments can be explained through the concept of wave-particle duality, which is a cornerstone of quantum mechanics [15–16]. According to this concept, particles such as electrons exhibit both particle-like and wave-like properties. When electrons pass through a crystalline structure, they interfere with each other in a manner similar to waves, creating a pattern of constructive and destructive interference that can be observed and measured.

The electron diffraction experiment was conducted within a glass bulb with a specified radius of 65 mm. The diffraction patterns for the first-order ring were observed and measured across varying voltages, yielding data as presented in Tables 1 and 2. Table 1 provides diameter measurements for the first-order ring at voltages ranging from 4.0 kV to 6.5 kV.

Table 1 – Voltage levels ranging from 4.0 kV to 6.5 kV and corresponding measurements of the first-order ring's diameter

Voltage V, *kV*	Inner Diameter, ±0.05 *mm*	Outer Diameter, ±0.05 *mm*
4.0	28.78	36.51
	50.15	61.11
4.5	21.03	30.98
	46.74	55.48
5.0	24.68	30.28
	42.75	50.12
5.5	22.31	27.73
	41.02	46.13
6.0	21.34	24.97
	38.12	43.88
6.5	21.01	24.75
	35.14	42.02

It is imperative to note that the diameter measurements were obtained using a Vernier caliper in a controlled environment. The precision of the measurements, coupled with the systematic variation of voltage, provides a comprehensive dataset for the analysis of electron diffraction behavior within the specified experimental setup.

Table 2 – Voltage levels ranging from 7.0 kV to 9.9 kV and corresponding measurements of the first-order ring's diameter

Voltage V, *kV*	Inner Diameter, ±0.05 *mm*	Outer Diameter, ±0.05 *mm*
7.0	19.47	25.02
	34.05	39.15
7.5	19.04	20.14
	32.38	36.75
8.0	17.15	19.46
	31.13	35.38
8.5	17.41	19.06
	31.14	34.98
9.0	17.11	20.05
	28.72	33.45
9.5	16.63	17.65
	26.98	32.15
9.9	16.75	18.15
	27.03	30.03

The calculated wavelength is crucial for understanding the interference patterns observed in the experiment, as it allows for the application of Bragg's law to determine the interplanar spacing of the crystalline structure being used. In the described experiment, a diffraction tube along with the requisite equipment was utilized to explore the wave-like characteristics of particles, specifically electrons. The experiment hinged on the principle of electron diffraction, where electrons demonstrate wave behavior when passed through a crystalline structure, such as graphite.

Each entry includes both inner and outer diameter values, with a precision of ±0.05 mm. Notable variations in diameter are observed with changes in voltage, indicating the sensitivity of the diffraction pattern to applied electrical potentials. Similarly, Table 2 details diameter measurements for the first-order ring at higher voltages, ranging from 7.0 kV to 9.9 kV. The precision of ±0.05 mm is maintained for both inner and outer diameter values. Again, the data underscores the impact of increased voltage on the dimensions of the diffraction ring.

Table 3 – The wavelength of the electrons under a certain acceleration voltage

Voltage U_A, *kV*	Wavelength, *pm*	The error of wavelength, *pm*
4.0	19.19	0.127
4.5	18.18	0.130
5.0	17.34	0.114
5.5	16.53	0.113
6.0	15.76	0.110
6.5	15.14	0.106
7.0	15.03	0.103
7.5	15.16	0.098
8.0	13.72	0.097
8.5	13.28	0.096
9.0	13.03	0.085
9.5	12.51	0.081
9.9	12.34	0.077

The dataset reveals a consistent trend wherein as the acceleration voltage increases, the electron wavelength decreases. This relationship is pivotal for understanding the behavior of electrons under varying electrical potentials. The associated error values underscore the meticulous nature of the measurements, ensuring the accuracy of the reported electron wavelengths.

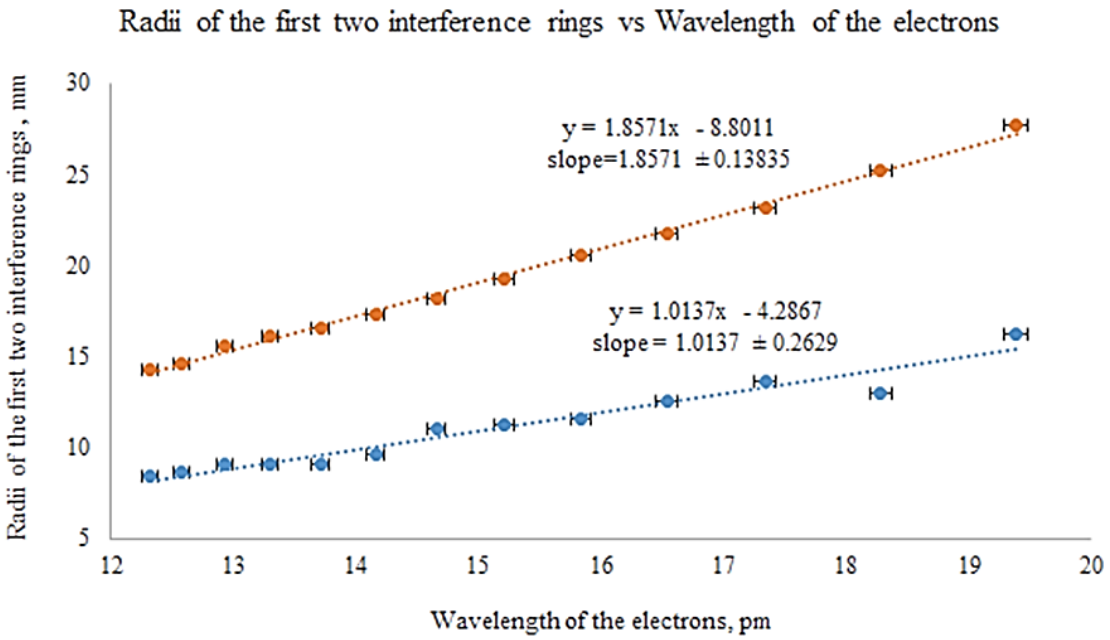

Figure 2 – Diameters of the initial two diffraction rings compared to the electron wavelength

These findings contribute to the broader comprehension of electron dynamics and wave-particle duality within the experimental framework.

The wavelength data, coupled with the associated errors, serves as a valuable resource for further analysis, theoretical modeling, and the advancement of knowledge in the field of electron diffraction studies.

As it can be seen, we observed some sort of unexpected results. We got values half as much as expected. Furthermore, according to the results of this experiment, the value of d_1 is closer to the theoretical value of d_2 and the value of d_2 is closer to the theoretical value of d_3. We obtained results as if we were measuring the radii of second and third visible diffraction rings. It might be possible if the first ring was much smaller than the second and the third rings.

The brightness of incident light could have potentially worsened the situation so that we could not clearly see the first diffraction ring.

If we treat the experimental value of d_1 as the theoretical value of d_2 and the experimental value of d_2 as the theoretical value of d_3, we can conclude that the experiment was conducted successfully. However, the error of d_1 is comparable with the calculated value.

This is because data points for d1 are not within the desired margin so that they would have a good linear fit with a small slope error. It possibly might have been the result of systematic error in measuring diffraction rings' radii because those diffraction rings have very blurry boundaries and precisely measuring the inner and outer radii of the first diffraction ring is difficult for small values. This explains why d1 has a greater error than d_2.

We can mitigate the issue with radii measuring if we will use a sort of automatic measuring system that would easily measure inner and outer radii without cognitive biases that humans have. Also changing configurations so that diffraction rings are easier to measure can improve the situation with the error of d_1.

4. Conclusions

In a broader context, the success of the experiment hinges on the assumption that the measured parameters correspond to interplanar spacings d_2 and d_3, while the diffraction ring associated with d1 may have been sufficiently small to escape detection. The heightened brightness of the incident light potentially exacerbated this situation. Considering the possibility of overlooking the first diffraction ring, the derived values suggest that d_2 is 128.24±33.26 pm and d_3 is 70.00±5.21 pm. In comparison, the theoretical values for d_2 and d_3 are 123 pm and 80 pm, respectively. Remarkably, the experiment's results fall within an acceptable range, considering the inherent uncertainties.

To address the error in measuring diffraction ring radii, implementing an automated system is recommended, offering a potential solution by minimizing human-induced biases. Additionally, a careful reassessment and optimization of the experimental setup configurations are essential. Identifying ideal conditions under which diffraction rings are more easily measurable can significantly enhance the precision and reliability of the experimental outcomes. These considerations underscore the continuous need for refinement in methodology to ensure the accuracy of results and contribute to the advancement of scientific knowledge in the field.

References

1. Multiple Bragg diffraction in opal-based photonic crystals: Spectral and spatial dispersion / I.I. Shishkin, M.V. Rybin, K.B. Samusev, V.G. Golubev, M.F. Limonov // Physical Review B. — 2014. — Vol. 89. — P. 035124. https://doi.org/10.1103/PhysRevB.89.035124
2. Photonic Crystals: Molding the Flow of Light / J.D. Joannopoulos, S.G. Johnson, J.N. Winn, R.D. Meade. — Princeton, USA: Princeton University Press, 2018. — 305 p.
3. Optical Properties of Photonic Crystals / K. Sakoda. — New York, USA: Springer, 2004. — 258 p.
4. Optical Properties of Photonic Structures: Interplay of Order and Disorder / M.F. Limonov, R.M. De La Rue. — Florida, USA: CRC Press, Taylor & Francis Group, 2012. — 528 p.
5. Crystallographic Analysis of Graphite by X-Ray Diffraction / A.N. Popova // Chemistry. — 2017. — Vol. 60. No. 9. — P. 361-365. https://doi.org/10.3103/S1068364X17090058

6. Photonic band gaps structure properties of two-dimensional function photonic crystals / J. Lachter, R.H. Bragg // Physical Review B. — 2017. — Vol. 89. — P. 61 – 66. https://doi.org/10.1016/j.physe.2017.01.028
7. XRD Characterization of the Structure of Graphites and Carbon Materials Obtained by the Low-Temperature Graphitization of Coal Tar Pitch / Ch.N. Barnakov, G.P. Khokhlova, A.N. Popova, S.A. Sozinov, Z.R. Ismagilov // Eurasian Chemico-Technological Journal. — 2015. — Vol. 17. — P. 87–93.
8. Photonic Crystals: Molding the Flow of Light / J.D. Joannopoulos, S.G. Johnson, J.N. Winn, R.D. Meade. — Princeton, USA: Princeton University Press, 2008. — 305 p.
9. Inhibited spontaneous emission of quantum dots observed in a 3D photonic band gap / M.D. Leistikow, A.P. Mosk, E. Yeganegi, S.R. Huisman, A. Lagendijk, W.L. Vos // Physical Review Letters. — 2011. — Vol. 107, No. 19. — P. 193903. https://doi.org/10.1103/PhysRevLett.107.193903
10. Observation of sub-Bragg diffraction of waves in crystals / S.R. Huisman, R.V. Nair, A. Hartsuiker, L.A. Woldering, A.P. Mosk, W.L. Vos // Physical Review Letters. — 2012. — Vol. 108, No. 8. — P. 083901. https://doi.org/10.1103/PhysRevLett.108.083901
11. Diffraction of light from thin-film polymethyl methacrylate opaline photonic crystals / S. G. Romanov et al // Physical Review Letters. — 2001. — Vol. 63, No. 5. — P. 056603. https://doi.org/10.1103/PhysRevE.63.056603
12. Polarized light coupling to thin silica-air opal films grown by vertical deposition / A. V. Baryshev et al. // Physical Review Letters. — 2007. — Vol. 76, No. 1. — P. 014305. https://doi.org/10.1103/PhysRevB.76.014305

Information about authors:

Nurzhan Dosaev – Master Student, Physics Department, M. Kozbayev North Kazakhstan University, 13 Internatsionalnaya str., Petropavlovsk, Kazakhstan, dosayev.n@gamil.com
Gulzhan Tulekova – Master Student, Physics Department, M. Kozbayev North Kazakhstan University, 13 Internatsionalnaya str., Petropavlovsk, Kazakhstan, gulzhan.tulekova@bk.ru

Author Contributions:

Nurzhan Dosaev – concept, methodology, data collection, analysis, visualization, drafting.
Gulzhan Tulekova – resources, testing, modeling, interpretation, editing, funding acquisition.

Received: 8 September 2023
Revised: 25 September 2023
Accepted: 28 September 2023
Published: 28 September 2023

Technobius, 2023, 1(4), 0005c, DOI: https://doi.org/10.54355/tbusphys/1.4.2023.0005c

Technobius Physics

https://technobius.kz/

e-ISSN 2789-7338

Corrigendum Notice: A corrigendum has been issued for this article and is included at the end of this document.

Post-Publication Notice

Corrigendum to "N. Dosaev and G. Tulekova, "Exploring the labyrinth of light: multiple Bragg Diffraction phenomena in face-centered cubic photonic crystals", tbusphys, vol. 1, no. 4, p. 0005, Sept. 2023. doi: 10.54355/tbusphys/1.4.2023.0005"

In the originally published version of this article, omissions were identified in the Methods section, leading to insufficient detail about the experimental setup and data processing procedures.
The following corrections have been implemented:
1. Section 2 (Methods):
- The updated text now specifies all experimental apparatus components, including manufacturers (SciTech Company, USA), connection setup, voltage ranges, safety elements, and measurement tools.
- The revised version also incorporates information about data analysis procedures, including the use of Bragg's law, linear regression of diffraction data, ANOVA for statistical significance testing, and error estimation methods (mean ± standard deviation).
2. Clarifications: The sequence of steps for configuring the apparatus, adjusting voltages, and collecting measurements has been elaborated to improve reproducibility.
Additionally, the reference: "Interstitials in graphite and disordered carbons / J. Lachter, R.H. Bragg // Physical Review B. — 1986. — Vol. 33. No. 12. — P. 8903." has been replaced with "Photonic band gaps structure properties of two-dimensional function photonic crystals / J. Lachter, R.H. Bragg // Physical Review B. — 2017. — Vol. 89. — P. 61 – 66. https://doi.org/10.1016/j.physe.2017.01.028".
These amendments do not alter the experimental results, discussion, or conclusions of the paper. They enhance methodological transparency and accuracy of reported procedures.

Published: 02.12.2024

Technobius Physics, 2023, 1(4), 0006, DOI: https://doi.org/10.54355/tbusphys/1.4.2023.0006

Technobius Physics

https://technobiusphysics.kz/

e-ISSN 3007-0147

Corrigendum Notice: A corrigendum has been issued for this article and is included at the end of this document.

Article

Experimental study of the influence of modified sulfur components on physical and mechanical characteristics of bitumen compositions

Tomiris Beisenbayeva[1,*], Anna Schmidt[2]

[1]School of Engineering and Digital Sciences, Nazarbayev University, 53 Kabanbay ave., Astana, Kazakhstan
[2]Faculty of Mechanical engineering, University of Applied Sciences Duesseldorf, 156 Münsterstraße st., Duesseldorf, Germany
*Correspondence: tbeisenbayeva@mail.ru

Abstract. In this research work, the physical, mechanical and performance characteristics of bituminous binder 90/130 before and after its modification with sulfur in the proportions of 10%, 30% and 50% of the binder weight were analyzed. Experimental results showed the effect of sulfur content on the mechanical characteristics of bituminous binder. By elemental analysis of the spectra of modified bitumen binder samples, it was found that there were no significant chemical changes with increasing sulfur content. The formation of new chemical compounds was not revealed, which is confirmed by the absence of new characteristic peaks in the spectra. Analysis and comparison of the experimental data of softening temperature showed an insignificant influence of the liquid heating rate on the concentration of the modifying agent. However, the increase of sulfur concentration more than 10% in the modified bitumen leads to an increase in softening temperature. This is due to the formation of denser structure and increase in viscosity of bitumen with increasing amount of sulfur in the system. Thus, the presence of sulfur as a dispersed phase in polymer bitumen has a natural effect on the mechanical characteristics of sulfur asphalt concretes, leading to an increase in their mechanical properties with increasing sulfur content.

Keywords: bituminous binders, modified bitumen, sulfur, ring and ball method, softening point, penetration.

1. Introduction

Modern highways, especially those subjected to significant dynamic loads, as well as airfield runways and cargo areas, require high quality standards for their asphalt concrete pavements [1]. Petroleum bitumens, which are dispersed colloidal systems of complex chemical composition, are used as road binders. To improve the quality and durability of road surfaces, modified road binders are now widely used [2]. The modification process is aimed at improving the properties of bitumen by combining it with special components.

Nowadays, not pure bitumen, but modified with different components, the main difference of which is higher performance characteristics and qualities, is used quite actively in the field of construction [3-6].

Studies on the use of sulfur as a modifying constituent in bituminous binders have started relatively recently and are not fully understood [7]. Crystalline sulfur, produced as are product in the oil and gas industry, it's an available resource that, when in solid state, is non-toxic and has high chemical resistance in a variety of aggressive industrial environments [8].

The authors of the works revealed [9, 10] that sulfur not only serves as a mixture filler, but also acts as a stabilizer of bitumen mixture. Another work presents that the addition of sulfur content in paving materials above 30%, with the correct design and methodology of bitumen binder modification, leads to effective stabilization of these materials [9].

According to standard normative documents [11], one of the key indicators of binders are the values of softening point and brittleness temperature. The working range of a binder is defined as the difference between the brittleness temperature (usually below -17°C) and the softening point (usually above +43°C). In this range, the substance is in a visco-plastic state characterized by moderate plasticity without brittleness and the ability to retain shape without fluidity under small shear loads. Thus, materials based on such a binder have the required consumer properties, such as moderate ductility and shear stability, over the operating temperature range.

Due to the need to ensure the stability of bituminous binder properties at all stages of the technological process there is a need to improve a set of methods for assessing its quality.

This paper presents the results of research into one of the most effective directions in road construction - modification of petroleum road bitumen and obtaining sulfur asphalt concrete on their basis.

2. Methods

In this study, a consecutive series of experiments was carried out in order to identify in detail the nature of interaction between gray and oil bitumen. The object of the study was oil road bitumen 90/130 produced by Promstroybitum, LLP, corresponding to [11].

In the manufacture of sulfur-bitumen binder was used granulated crystalline sulfur according to [12] in proportions of 10%, 30% and 50% of bitumen weight. The process of modification was carried out by heating on a water bath to 100^{o}C of pure bitumen grade 90/130 and adding sulfur and with careful and continuous stirring with a propeller mixer at a speed of 100 rpm for 90 min. Multi-element analysis of a wide range of matrices of modified bitumen was carried out on a Rigaku EDXRF spectrometer (Japan), which use X-rays in the energy range 1-65 eV and photoelectric effect to determine the elemental composition.

The study of mechanical properties of modified bitumen was based on the study of mechanical properties of the base sample of bitumen 90/130 relative to the samples with the addition of sulfur.

To determine the thermal sensitivity and resistance of the sample of bitumen 90/130 to deformation, studies of its softening temperature (T_S) were carried out on the automatic equipment B072 "Automatic apparatus ring and ball" of the company "Matest" (Italy). Two chromium-plated rings of step form were filled with 6 g of base bitumen without modifier each. For the purpose of additional fixation two centering rings and two steel balls Ø9.5 mm. each were placed on top of them. The finished samples were mounted in a special brass frame for immersion in a beaker made of pyrexerglass, i.e. the medium. Freshly distilled cooled distilled water of 600 ml volume was used as a thermoregulating medium. The process of water heating not exceeding 80^{o}C was carried out using an integrated glass-ceramic heating surface providing a heating rate of 5°C/min. in accordance with the requirements of [11]. Uniform heating was provided by the built-in magnetic stirrer with electronic speed controller, capable of providing rotation in the range from 0 to 160 rpm. The temperature sensor connected to the B072 apparatus was inserted in the center of the brass frame, providing accurate recording of the temperature change of the medium. Two integrated laser sensors were used to record the ball drop moment used to determine the softening temperature. These were placed on either side of a beaker containing distilled water. The difference in T_S between the base and modified bitumen is not more than 1°C, which is within the normalized measurement error.

Studies of specific viscosity of modified bitumen were carried out on penetrometer B056-02 KIT of "Matest" (Italy). Penetration was subjected to modified bitumen with a mass of 1500 g., preheated in a steam bath to 100^{o}C. Penetrometer equipped with digital micrometric adjustment was automatically fixed at zero position at the boundary of the needle and modified bitumen touching. Special 50 g and 100 g weights were mounted on the penetrometer to ensure vertical penetration of the standard needle. A magnetic controller with an electronic digital programmable timer, automatically releasing the plunger head with the specified mass, ensured free fall of the needle during the 5-second test. Depth, penetration time and sample temperature were recorded automatically.

To verify the reliability and reproducibility of the experimental results, all measurements were performed in triplicate. The data were statistically analyzed using OriginPro 2023 and Python (SciPy and NumPy libraries). The mean, standard deviation, and coefficient of variation (CV) were calculated for each experimental series to assess consistency. Differences in softening temperature and penetration depth between modified and base samples were evaluated using one-way analysis of variance (ANOVA). A significance level of $p < 0.05$ was used to determine statistical significance. Linear regression analysis was also applied where applicable to assess the correlation between sulfur content and bitumen properties.

3. Results and Discussion

In order to control the process of bituminous binder modification and to determine the chemical composition of bitumen 90/130 after modification with sulfur in the proportions of 10%, 30% and 50% of the initial sample weight, elemental analysis was carried out on a Rigaku EDXRF spectrometer in the energy range from 4 to 23 eV (Figure 1).

Graph 1 shows the spectra of elemental analysis of bitumen 90/130 before and after modification with sulfur 10%, 30% and 50%. In the obtained spectra intense characteristic peaks of bitumen 90/130 binder at 17 eV and 18 eV corresponding to stretching vibrations of C-H noodles in CH_2 elements are noticeable. These peaks indicate the presence of a high concentration of arene in bitumen binder [13].

The first observed peak around 4.5 eV corresponds to deformation vibrations of CH_2 elements in alkane pairs. Three consecutive peaks with energies of 4.6 eV, 5.0 eV and 5.2 eV indicate out-of-plane vibrations of CH and also indicate the presence of arene compounds. These results are in agreement with previous studies [13], confirming the structural features and composition of the bituminous binder.

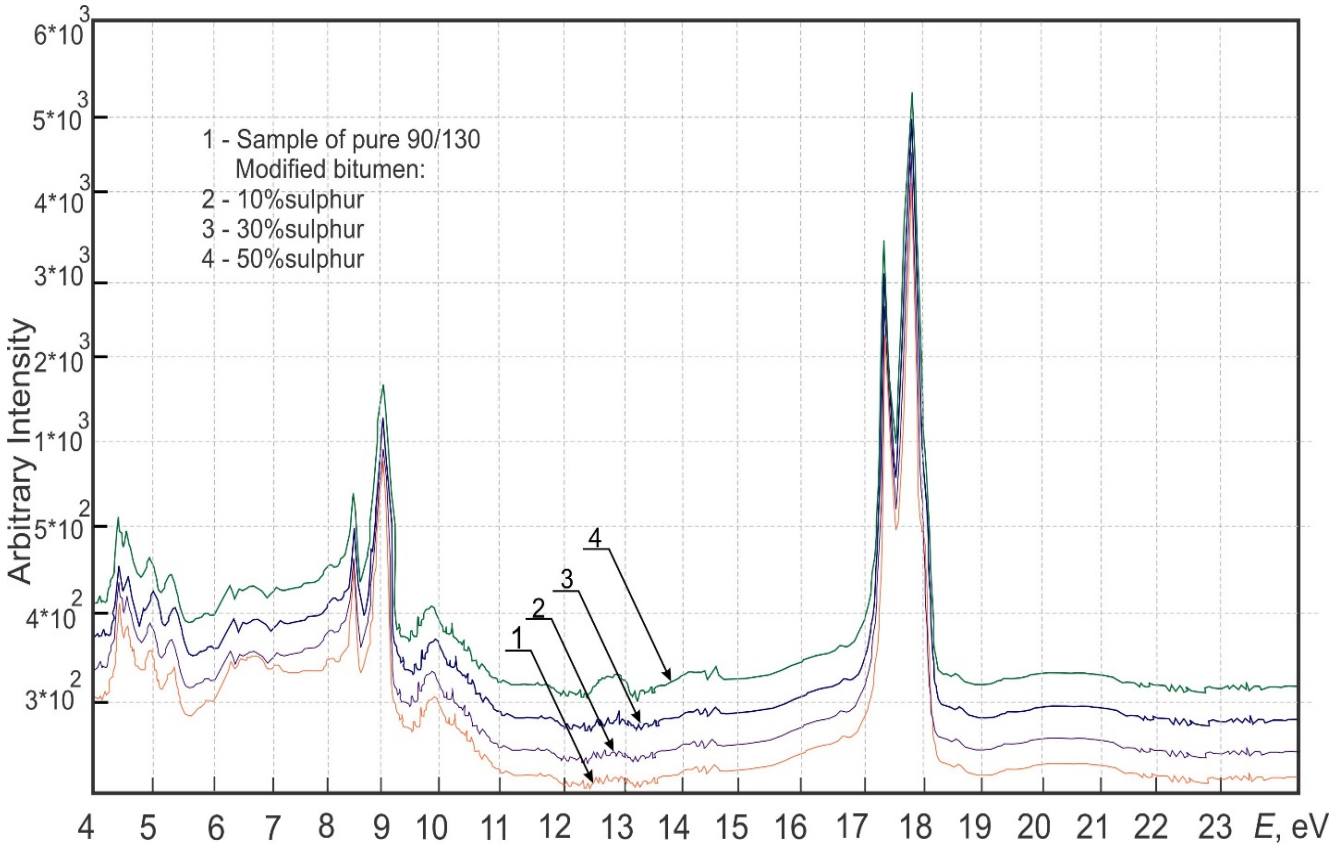

Figure 1 – Elemental analysis of a wide range of modified bitumen: 1 – Pure 90/130; 2 – modified bitumen with 10% sulphur; 3 – modified bitumen with 30% sulphur; 4 – modified bitumen with 50% sulphur

Further analysis of the spectra demonstrates an insignificant change in intensity at energies of 6.3 eV, 6.6 eV and 9.7 eV. The absence of significant peaks in these regions indicates that the modification of bituminous binder 90/130 does not lead to significant changes in its chemical composition. In other words, new chemical compounds formed due to the interaction of sulfur and oil bitumen were not detected. Similar results were obtained earlier in other studies [14], which confirms the continuity of this phenomenon. The intense peaks found around 8.5 eV and 9 eV correspond to the strain vibrations $\delta(CH_3)$ and $\delta(CH_2)$, respectively. These maxima are characteristic of saturated hydrocarbons, paraffins, and oils.

The maximum at 9.9 eV corresponds to stretching vibrations of C=C noodles; this feature is observed both in the spectra of the original sample bitumen 90/130 and in the spectra of sulfur-modified bitumen. The structural complexity of this band indicates the extensive presence of arene elements in the bitumen composition, including asphaltenes and other components [15].

When analyzing the spectra, it was also found that both the sample of the original bitumen 90/130 and the sample of modified bitumen with the addition of 10% sulfur contain bound water. This is confirmed by the presence of bands with peaks at 19 eV and 20 eV, which shows to stretching vibrations of the oxygen-hydrogen bond in hydroxyl groups involved in the formation of intermolecular hydrogen bonds. However, for samples with 30% and 50% sulfur content, these peaks are less intense, indicating less water. This suggests a potential improvement in performance properties, such as frost resistance, for bituminous binders with 30% and 50% sulfur content.

The results of the study of physical and mechanical properties of the modified binder indicate the effect of changing the concentration of sulfur on all analyzed characteristics of the binder. At the same time, the analysis of concentration dependences confirms the linear relationship between the sulfur concentration and the relative change in these properties.

Figure 2 shows the temperature dependence of the heating rate of the medium, demonstrating that increasing sulfur concentration leads to an increase in the Ts at all heating rates. The Ts is indicated as the average value of temperatures at a fixed rate at which two disks soften sufficiently for each ball wrapped with binder to fall a distance of 25 mm. The analysis of the results shows that varying the heating rate within 0.5 °C causes an error in the Ts measurement between 1.0 and 1.5 °C.

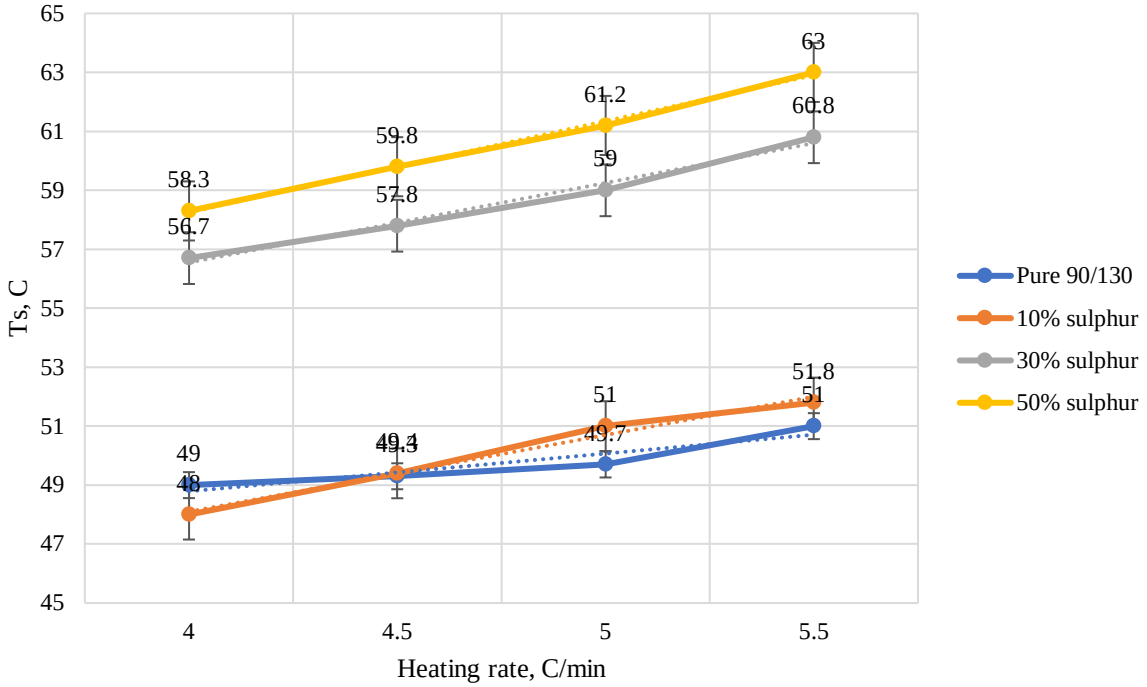

Figure 2 – Effect of medium heating rate on softening point of bitumen 90/130 before and after modification

From the graph 2 shows that the initial sample of bituminous binders grade 90/130 did not show a significant effect on the range of operating temperatures. However, at a concentration of sulfur not exceeding 10%, there is a decrease in softening temperature by 10%. This effect can be explained by the insufficient amount of sulfur formed and its low molecular weight, which does not contribute to the formation of a spatial mesh of the polymer, improving the working temperature range. When increasing the concentration of sulfur as a filler, the amount of formed mixture increases significantly, which leads to a marked increase in the viscosity of the system and, consequently, an increase in the softening temperature. It is worth noting that when introducing crystalline sulfur into bitumen 90/130 in the amount of 10%, 30% and 50% of the mass of the binder, the physical and chemical parameters meet the requirements of RK 218-145-2019.

One of the important parameters of physical and mechanical properties of binders is the measure of resistance under gravity. Studies on the effect of temperature on the penetration depth at 25°C of binders can be considered optimal, because such data allow us to evaluate the behavior of the material under conditions of comfortable temperature, which can be significant in the design and use of materials in different climatic zones [16].

To evaluate the dynamic viscosity of modified bitumen, we conducted studies aimed at revealing the dependence of penetration depth on temperature when adding weights weighing 50 g and 100 g, the data of which are shown in Figures 2 - 3.

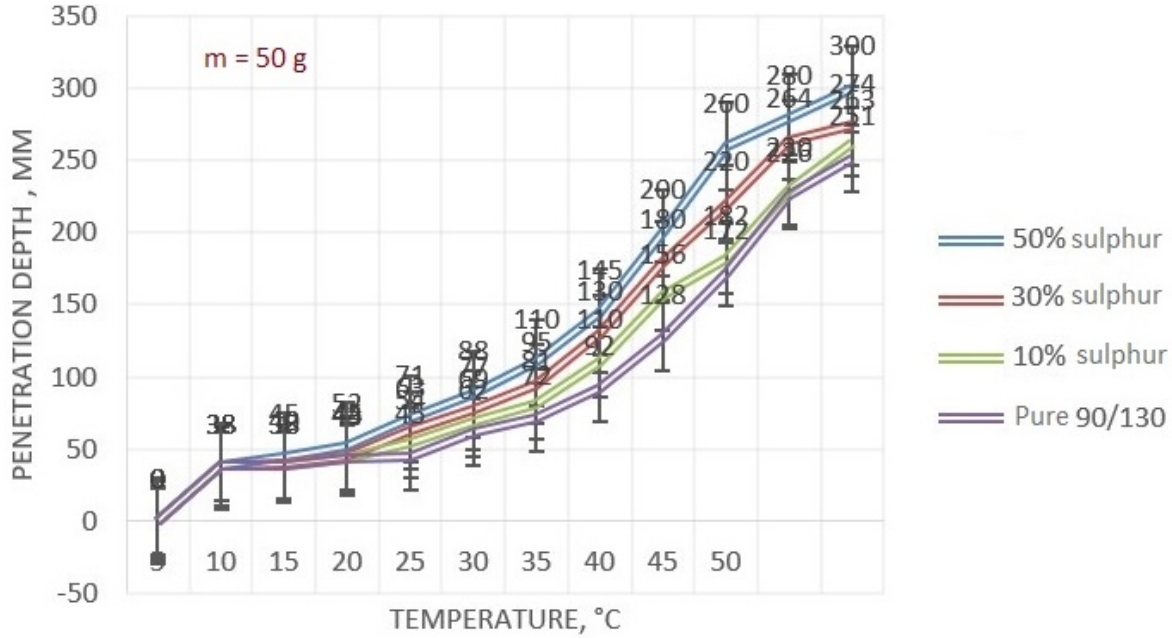

Figure 3 – Dependence of penetration depth on temperature of bitumen 90/130 before and after modification with additional mass of 50 g

Figure 3 shows the results of the analysis, which indicate that the changes in the properties of sulfur-bitumen binder associated with an increase in sulfur content. Note that to a large extent such changes are due to the presence of an additional dispersed phase due to physically free sulfur, which significantly affects the viscosity of the materials. Diagram 3 shows that at a standard temperature of 25°C and a mass of 50 g. the depth of penetration of the needle in the original sample of bitumen grade 90/130 is less than in the modified samples with the addition of sulfur. It is observed that the penetration depth increases with increasing sulfur concentration (10%, 30% and 50% of bitumen mass). This indicates an increase in the plasticity and softening of the material with increasing penetration, indicating a decrease in its brittleness. The experimental data in Figure 3 indicates that the effect of sulfur, which has a melting point of 120°C, becomes more prominent as the operating or testing temperature increases, which is consistent with the pattern of increasing its effect on material properties.

In order to determine the viscosity more accurately, we conducted an experiment at 100 g and the results are shown in Figure 4. The analysis of the obtained data shows that when increasing the temperature of sulfur-bitumen binder and increasing the additional load there is a slight increase in the depth of penetration of the needle into the bitumen. Consequently, we can conclude that the additional external load practically does not affect the increase in viscosity of bitumen 90/130 before and after modification with sulfur. It is worth noting that with increasing temperature in the range from 30°C - 50 °C penetration depth increases sharply, which indicates increased plasticity properties of pure and modified bitumen 90/130.

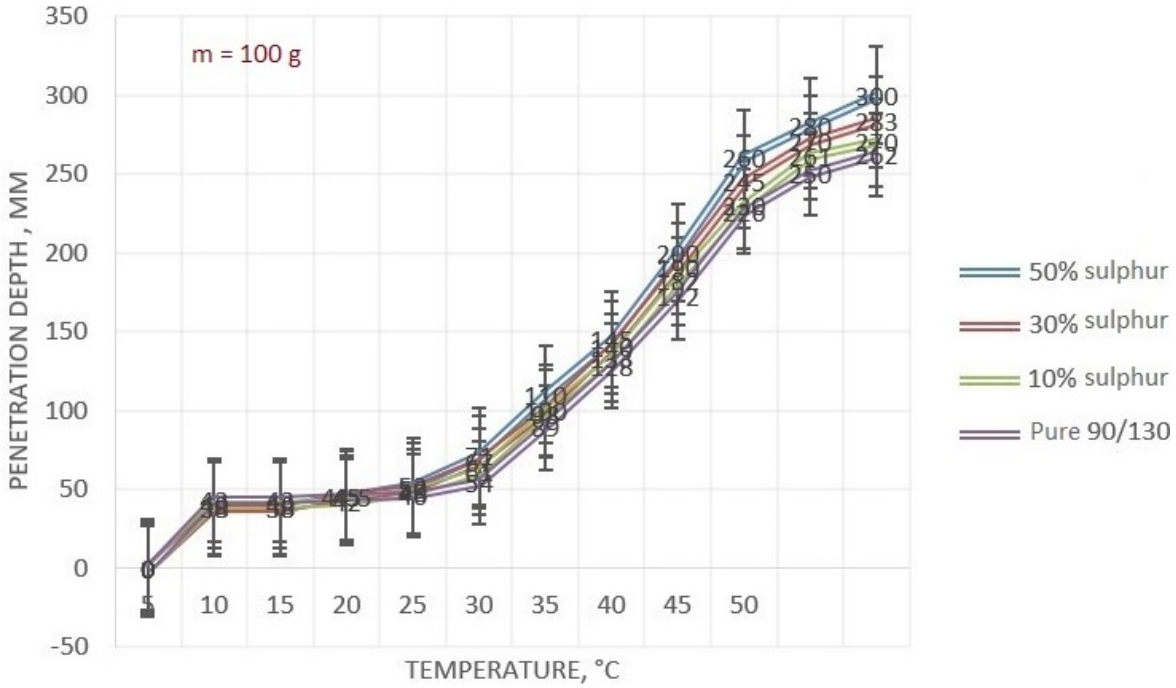

Figure 4 – Dependence of penetration depth on temperature of bitumen 90/130 before and after modification with additional mass of 100 g

4. Conclusions

In this work were investigated physical-mechanical and performance indicators of bituminous binder 90/130 before and after modification with sulfur in proportions of 10%, 30% and 50% of the binder weight. At elemental analysis of spectra of sulfur-modified bitumen binder samples no noticeable chemical changes were revealed. Increasing the mass fraction of sulfur from 10% to 50% in the binder bitumen 90/130 did not lead to the formation of new chemical compounds, which is confirmed by new characteristic peaks. Note that the positions of the main maxima of the recorded spectra did not differ significantly.

Analysis and experimental comparison of softening temperature allowed to reveal insignificant influence of liquid heating rate from the concentration of modifying component. Increase of sulfur concentration more than 10% in the modified bitumen leads to an increase in softening temperature. This is explained by an increase in the amount of sulfur in the system, which causes the formation of a denser structure and an increase in the viscosity of bitumen.

It is revealed that the presence of sulfur as a dispersed phase in bitumen has a regular effect on the mechanical characteristics of sulfur asphalt concretes: there is an increase in mechanical properties with increasing sulfur content.

References

1. Method research on evaluation standard of pavement ride quality / X. Zhou, B. Sun, Z. Chen, L. Sun // Tongji Daxue Xuebao/Journal of Tongji University. — 2007. — Vol. 35, No. 2. — P. 213–217.

2. The Modified Composite Binder for Cement-Concrete Road Surfaces / M.M. Kosukhin, A.M. Kosukhin // IOP Conference Series: Materials Science and Engineering. — 2018. — Vol. 463, No. 4. — Article number 042036. https://doi.org/10.1088/1757-899X/463/4/042036
3. Effect of storage stability on chemical and rheological properties of polymer-modified asphalt binders for road pavement construction / L. Zani, F. Giustozzi, J. Harvey // Construction and Building Materials. — 2017. — Vol. 145. — P. 326–335. https://doi.org/10.1016/j.conbuildmat.2017.04.014
4. Changes of component and property of pitch road binder modified by rubber during ageing / M.-L. Jin, A.-Z. Feng, M.-R. Shi, X.-G. Chen, C.-Y. Zhang, Y.-H. Li // Journal of Fuel Chemistry and Technology. — 2000. — Vol. 28, No. 2. — P. 188.
5. Application of bio-resin in road materials: Rheological and chemical properties of asphalt binder modified by lignin-phenolic resin / Y. Li, C. Lv, P. Cheng, Y. Chen, Z. Zhang // Case Studies in Construction Materials. — 2023. — Vol. 18. — P. e01989. https://doi.org/10.1016/j.cscm.2023.e01989
6. Assessment of temperature susceptibility for rubber granulate modified road asphalt binders considering impact of aging / M. Słowik, D. Wisniewski, M. Bilski, M. Mielczarek. 2018. — Vol. 222. — P. 01016. https://doi.org/10.1051/matecconf/201822201016
7. Modification of Inclusions by Rare Earth Elements in a High-Strength Oil Casing Steel for Improved Sulfur Resistance / X. Jiang, G. Li, H. Tang, J. Liu, S. Cai, J. Zhang // Materials. — 2023. — Vol. 16, No. 2. — Article number 675. https://doi.org/10.3390/ma16020675
8. Evaluation research and development suggestion on the low-carbon transformation of regional industry: Take Quangang District as an example / H. Gan, Y. Jiang, H. Qi, H. Wuhong, Y. Cai // IOP Conference Series: Earth and Environmental Science. — 2020. — Vol. 467, No. 1. — Article number 012178. https://doi.org/10.1088/1755-1315/467/1/012178
9. Evaluation of Mixture Performance and Structural Capacity of Pavements Using Shell Thiopave / N. Tran, A. Taylor, D. Timm, M. Robbins, B. Powell, R. Dongre // NCAT Report. — 2010. — Vol. 10, No. 5. — P. 1597.
10. Field performance experience of Sulfur Extended Asphalt (SEA) pavement in Saudi Arabia / A. Alyami, L.S. Toyogon // Advances in Materials and Pavement Performance Prediction II - Contributions to the 2nd International Conference on Advances in Materials and Pavement Performance Prediction, AM3P 2020. — 2020. — Article number 172260. https://doi.org/10.1201/9781003027362-1
11. GOST 22245–90 Viscous petroleum road bitumen. — 1991.
12. GOST 127.1-93 Sulphur for industrial use. — 1994.
13. A DFT study of infrared spectra and Monte Carlo predictions of the solvation shell of Praziquantel and β-cyclodextrin inclusion complex in liquid water / C.X. De Oliveira, N.S. Ferreira, G.V.S. Mota // Spectrochimica Acta - Part A: Molecular and Biomolecular Spectroscopy. — 2016. — Vol. 153. — P. 102–107. https://doi.org/10.1016/j.saa.2015.08.011
14. Structure Formation and Phase Composition of Sulfur-Bitumen Systems / V. Gladkikh, E. Korolev, D. Husid // Materials Science Forum. — 2016. — Vol. 871. — P. 110–117. https://doi.org/10.4028/www.scientific.net/MSF.871.110
15. Examination of bitumen-polymers interaction / D.A. Ayupov, L.I. Potapova, A.V. Murafa, V.H. Fakhrutdinova, Yu.N. Khakimullin, V.G. Khozin // News of Kazan State University of Architecture and Construction. — 2011. — Vol. 15. — P. 140–145.
16. EN 1426:2015 Bitumen and bituminous binders — 2015.

Information about authors:

Tomiris Beisenbayeva – Master Student, School of Engineering and Digital Sciences, Nazarbayev University, 53 Kabanbay ave., Astana, Kazakhstan, tbeisenbayeva@mail.ru
Anna Schmidt – Master Student, Faculty of Mechanical engineering, University of Applied Sciences Duesseldorf, 156 Münsterstraße st., Duesseldorf, Germany, as0041526@gmail.com

Author Contributions:

Tomiris Beisenbayeva – concept, methodology, resources, data collection, testing.
Anna Schmidt – modeling, analysis, visualization, interpretation, drafting, editing, funding acquisition.

Received: 02.10.2023
Revised: 23.10.2023
Accepted: 23.10.2023
Published: 25.10.2023

Technobius Physics, 2023, 1(4), 0006c, DOI: https://doi.org/10.54355/tbusphys/1.4.2023.0006c

Technobius Physics

https://technobiusphysics.kz/

e-ISSN 3007-0147

Corrigendum Notice: A corrigendum has been issued for this article and is included at the end of this document.

Post-Publication Notice

Corrigendum to "T. Beisenbayeva and A. Schmidt, "Experimental study of the influence of modified sulfur components on physical and mechanical characteristics of bitumen compositions", tbusphys, vol. 1, no. 4, p. 0006, Oct. 2023. doi: 10.54355/tbusphys/1.4.2023.0006"

In the originally published version of this article, omissions were identified in the Methods section regarding the statistical analysis applied to the experimental data. The following corrections have been made:

1. Section 2 (Methods):

- The updated version explicitly states that all measurements were conducted in triplicate to ensure reliability.
- Details on the statistical analysis have been added, specifying the use of OriginPro 2023 and Python libraries (SciPy, NumPy) for calculating mean values, standard deviations, coefficients of variation, one-way ANOVA ($p < 0.05$), and linear regression analyses to assess the relationship between sulfur content and mechanical properties.

2. Minor textual clarifications were made to improve the reproducibility of the experimental procedure.

Additionally, the following references have been updated:

– "Modified binders: an underexploited road maintenance tool / T. Hoban // Highways Croydon. — 1987. — Vol. 55, No. 3. — P. 1926." has been replaced with "The Modified Composite Binder for Cement-Concrete Road Surfaces / M.M. Kosukhin, A.M. Kosukhin // IOP Conference Series: Materials Science and Engineering. — 2018. — Vol. 463, No. 4. — Article number 042036. https://doi.org/10.1088/1757-899X/463/4/042036 ";

– "Casting sulfur pipe / I. Bencowitz // Industrial and Engineering Chemistry. — 1938. — Vol. 30, No. 7. — P. 759– 764" have been replaced with "Modification of Inclusions by Rare Earth Elements in a High-Strength Oil Casing Steel for Improved Sulfur Resistance / X. Jiang, G. Li, H. Tang, J. Liu, S. Cai, J. Zhang // Materials. — 2023. — Vol. 16, No. 2. — Article number 675. https://doi.org/10.3390/ma16020675";

– "The manufacture of industrial carbons from petroleum raw materials / C.A. Stokes // Preprints. — 1975. — Vol. 20, No. 2. — P. 387." have been replaced with "Evaluation research and development suggestion on the low-carbon transformation of regional industry: Take Quangang District as an example / H. Gan, Y. Jiang, H. Qi, H. Wuhong, Y. Cai // IOP Conference Series: Earth and Environmental Science. — 2020. — Vol. 467, No. 1. — Article number 012178. https://doi.org/10.1088/1755-1315/467/1/012178";

– "Field evaluation of sulfur-extended asphalt pavements / T.L. Beatty, K. Dunn, E. Harrigan, K. Stuart, H. Weber // Transportation Research Record. — 1987. — Vol. 1115. P. 116–170." have been replaced with "Field performance experience of Sulfur Extended Asphalt (SEA) pavement in Saudi Arabia / A. Alyami, L.S. Toyogon // Advances in Materials and Pavement Performance Prediction II - Contributions to the 2nd International Conference on Advances in Materials and Pavement

Performance Prediction, AM3P 2020. — 2020. — Article number 172260. https://doi.org/10.1201/9781003027362-1";
– "The Infrared Spectra of Complex Molecules. — Berlin, Germany: Springer Dordrecht, 1980. — 300 p." have been replaced with "A DFT study of infrared spectra and Monte Carlo predictions of the solvation shell of Praziquantel and β-cyclodextrin inclusion complex in liquid water / C.X. De Oliveira, N.S. Ferreira, G.V.S. Mota // Spectrochimica Acta - Part A: Molecular and Biomolecular Spectroscopy. — 2016. — Vol. 153. — P. 102–107. https://doi.org/10.1016/j.saa.2015.08.011".
These amendments do not affect the scientific results, discussion, or conclusions of the paper. They are intended to enhance methodological transparency and data reliability.

Published: 05.12.2024